Biomass Conversion and Biorefinery (2023) 13:12917–12933
https://doi.org/10.1007/s13399-022-02518-w

ORIGINAL ARTICLE

Comparative analysis of three kinds of extraction kinetic models of crude polysaccharides from *Codonopsis pilosula* and evaluate the characteristics of crude polysaccharides

Yonggang Wang[1] · Chenliang Wang[1] · Hongyan Xue[1] · Yongming Jin[1] · Mingjun Yang[1] · Feifan Leng[1]

Received: 12 August 2021 / Revised: 23 February 2022 / Accepted: 27 February 2022 / Published online: 19 March 2022

Abstract
In this study, the second-order model, Fick's second law of diffusion, and the Peleg model were used to evaluate the extraction kinetic model of polysaccharide (CPP) from *Codonopsis pilosula*. The characteristic functional groups, surface structure, and physical and chemical properties of CPP were analyzed by multi-spectroscopic and microscopic techniques. The results showed that the extraction process agreed well with the second-order model, Fick's second diffusion law, and Peleg model. Rheological tests showed that CPP exhibited different viscosity changes under different conditions (Solution viscosity was inversely proportional to temperature, time, etc.; proportional to polysaccharide concentration, Na^+ content, etc.). CPP was composed of molecular aggregates composed of small particles, with more pore structure and basically completely decomposed at 130 °C. The hypoglycemic study showed that CPP had a strong inhibitory effect on α-glycosidase than α-amylase. The morphology and subsequent structural features, anti-diabetic potential, and rheological properties of CPP were revealed to provide a theoretical basis for the development of pharmaceutical preparations or health food and functional food for the treatment of diabetes.

Keywords *Codonopsis pilosula* polysaccharide · Kinetics · Rheology, Hypoglycemic activity

1 Introduction

Botanical products are new favorites in many fields because of their low toxicity and easy degradation [1]. Most of the natural extracts are ubiquitous in the field of medicine [2]. Codonopsis is the dried plant root of *Codonopsis pilosula* (Franch.) Nannf, *C. pilosula* Nannf var. *modesta* (Nannf.) LT. Shen or *C. tangshen* Oliv, belonging to the genus *Codonopsis* of Campanulaceae. *C. pilosula* (CP), an authentic medicinal material, is mainly produced in areas with an altitude of 1560 to 3100 m in Gansu Province, China. It has many functions such as treating stomach weakness and is used in people's daily life. With the development of science and technology, the research on the chemical components of CP has been continuously deepened including the extraction technology, analysis methods, and isolation, purification, and structure identification of the chemical components. Polysaccharides were originally called immunostimulants [3], which were a type of natural polymer formed by connecting aldose or ketose via glycosidic bonds. Previous studies had reported that *C. pilosula* polysaccharides (CPP) had a wide range of biological activities, such as anti-fatigue [4], anti-virus [4], anti-oxidation [5], immune regulation [6], inhibition of tumor cell proliferation [7], promotion of apoptosis [7], promotion of blood coagulation [8], regulation of intestinal microbes [9], and prevention of neurodegenerative diseases [10]. Sulfation modification can improve the antioxidant and hepatoprotective activities of CPP [11] and has some application prospects in the development of new anti-coronavirus drugs and vaccines [12], etc. Polysaccharides also have good physical and chemical properties, good biocompatibility, and low toxicity, so they have been widely used as biomaterials in medical and biological fields [13].

Yonggang Wang and Chenliang Wang are co-first authors.

✉ Yonggang Wang
412316788@163.com

✉ Feifan Leng
lff0928@sina.com

[1] School of Life Science and Engineering, Lanzhou University of Technology, Langongping Road 287, Qilihe District, Lanzhou City 730050, Gansu Province, China

The extraction process is very important and indispensable in the production of Chinese herbal medicine, and its core is to use solvents to extract active ingredients from Chinese herbal medicines. The typical method generally used to extract medicinal plant polysaccharides is hot-water extraction, which belongs to the "green extraction method." Water extraction is also widely applied into the pharmacy industry due to its lower cost-effectiveness, high repeatability, simplified operation, and shorter extraction time producing more target compounds and lower energy input. To get the optimal extraction conditions to increase the yield, we try to establish a model to expound the interaction among extraction time, temperature, solid–liquid ratio, and particle size. In fact, mathematical modeling can simplify the process design and control to obtain the optimization condition and provide correct information for large-scale extraction and preparation [14]. Kinetic modeling is of great significance for understanding the complex diffusion, mass transfer, and thermodynamic parameters affecting extraction [15, 16]. Many material kinetic models for extracting polysaccharides from other traditional Chinese medicines have been reported before, such as two-point kinetic models [17], first-order models [18], two-parameter empirical models [19], and chemical kinetics and diffusion models based on Fick's law [20]. Most studies indicate that the two-stage rate model can best describe the dynamics of modern and traditional extraction techniques [21, 22]. Looking at the mathematical models of plant target component dynamics deduced and established by domestic and foreign researchers, they are all guided by the theory of mass diffusion and mass transfer. The granular structure of plant particle is derived from abstract assumptions such as spherical, quasi-spherical, and cylindrical, and then the equation is further simplified and revised. However, due to factors such as the tissue structure, hardness, and density, it is difficult to establish a universally applicable extraction kinetic model from plant tissues during the process of non-steady state diffusion and mass transfer of active ingredients.

Most of the studies on CPP focus on its activity and structure [4–6], while the studies on kinetic extraction models are relatively few. In this study, the effects of extraction factors such as temperature, the ratio of material to liquid, particle size, and extraction time on the yield of CPP were investigated. And the second-order rate model and Fick's second law and Peleg model were fitted to extract the kinetic equation of CPP. To determine the best model suitable for industrial applications, the parameters in each model were solved and compared to obtain the optimal hot-water extraction CPP kinetic model. These results in this study can provide valuable data for the pilot-scale design and industrial application of the CPP extraction process. At the same time, a preliminary study of the physical and chemical properties, rheological properties, hypoglycemic activity, and polysaccharide structure of CPP was carried out in combination with a variety of spectroscopic techniques. It has a certain guiding significance for the development and utilization of CPP.

2 Materials and methods

2.1 Material pretreatment and source

CP was produced in the local medicine market of Minxian, Dingxi City, Gansu Province, China. The surface sediment was washed with tap water, then washed several times with distilled water, dried in a drying oven (45 °C, 36 h), crushed, and sifted through 40, 60, and 80 mesh, respectively. The particles with uniform particle size were selected as experimental materials.

2.2 CPP preparation

The CPP was extracted using the hot-water extraction method, and 5.0 g of the dried CP powder was weighed out and mixed with distilled water in a 100-mL conical flask. The extraction was carried out according to the pre-experimental requirements for extraction time, solid–liquid ratio, extraction temperature, and particle size. After the extraction, the crude extract was centrifuged at 4500 rpm for 15 min to separate the supernatant extract and solid residue (TD5A-WS, Changsha Xiangyi Centrifuge Instrument Co. Ltd., Hunan, China). After the supernatant was collected and concentrated to 1/5 volume, the concentrate was further mixed with ethanol with a final concentration of 80% (V/V) and precipitated at 4 °C for 24 h. The precipitate collection was used by the Sevag method [23] to remove protein 5 times. The upper liquid was dialyzed with 8000–10,000 Da dialysis bag for 24 h, and the crude polysaccharides were obtained by freeze-drying (SCIENIZ-18 N, Ningbo Biotechnology Co. Ltd., Ningbo, China).

$$\text{yield}(\%) = \frac{C \times V \times F}{M} \times 100 \quad (1)$$

where C denotes the concentration of polysaccharides (mg/mL); F denotes the dilution factor; V denotes the volume of extraction solution (mL); and M denotes the weight of CPP (g).

According to the abovementioned extraction process, the dynamics model was established based on the experimental data.

2.3 CPP kinetic model fitting analysis

To study the effect of experimental factors (solid-to-liquid ratio, extraction time, extraction temperature, particle size) on the yield of CPP, the solid to liquid ratio was set at 1:08, 1:10, 1:12, 1:14, and 1:16 (g/mL); the material particle size was chosen to 40 mesh (420 μm), 60 mesh (250 μm), and 80

Table 1 CPP water extraction conditions

Level	Factor			
	Time (T/min)	Temperature (°C)	Solid–liquid ratio (g/mL)	Particle size (μm)
1	10	40	8	420
2	20	50	10	250
3	30	60	12	180
4	40	70	14	
5	50	80	16	
6	60			
7	70			
8	80			

mesh (180 μm); the extraction temperature was given at 40, 50, 60, 70, and 80 °C; and the extraction time was set at 10, 20, 30, 40, 50, 60, 70, and 80 min. The extraction experiment was performed according to the combination shown in Table 1. The phenol–sulfuric acid method [24] was used to determine the polysaccharide content in each experiment.

The extraction process of polysaccharides is complicated. The essence is the mass transfer process of the effective components from the intracellular diffusion of the medicinal materials to the solvent, and the solute concentration in the particles decreases continuously with time, which is an unstable mass transfer process. The process is generally considered to have three steps:

(1) The solvent is mixed with CP particles, penetrates the particles, and dissolves the polysaccharides of CP (solvent penetration).
(2) The dissolved polysaccharide diffuses to the particle surface (internal diffusion).
(3) The polysaccharide moves from the surface of the particle to the main body of the solution diffusion (external diffusion).

In the abovementioned procession, the second step (internal diffusion) determined directly the yield of CPP. At this time, the particle size of CP, extraction temperature, solid to material ratio, and extraction time will all affect the internal diffusion efficiency. The following three kinetic models will be used to model the CPP extraction kinetics as shown in the following (Table 2).

2.3.1 Second-order rate model

The second-order rate model was applied to study the extraction kinetics of CPP. The second-order rate model can well explain the mass transfer mechanism of active components in the process of solid–liquid extraction [25, 26]. The dissolution rate of active components in CP granules can be expressed by the following equation:

$$\frac{dC_t}{dt} = k(C_s - C_t)^2 \tag{2}$$

where C_t is the concentration of the active ingredient in the extract at any time t (mg polysaccharide/100 g dry matter); C_s is the concentration of the active ingredient in the CP granule at any time t (mg polysaccharide/100 g dry matter); and k is the second-order extraction rate constant.

The initial and boundary conditions of Eq. (2) are given as follows: $t=0$, $C_t=0$, and $t=t$, $C=C_t$. According to this condition, the solution of Eq. (2) can be obtained as Eq. (3).

$$C_t = \frac{C_s^2 kt}{1 + C_s kt} \tag{3}$$

Transform the Eq. (2) to obtain the Eq. (3):

$$\frac{t}{C_t} = \frac{1}{kC_s^2} + \frac{t}{C_s} = \frac{1}{h} + \frac{t}{C_s} \tag{4}$$

In Eq. (4), h is the extraction rate of the active ingredient at the initial time. Equation (4) is deformed again to obtain the total polysaccharide concentration at any time t, and the expression is shown in Eq. (5).

$$C_t = \frac{1}{\left(\frac{1}{h}\right) + \left(\frac{t}{C_s}\right)} \tag{5}$$

In which, the extraction rate (h) of the active ingredient at the initial moment and the second-order extraction rate constant (k) in the saturated state could be calculated through the slope and intercept of the linearity curve that plots t by t/C_t.

2.3.2 Fick's second law model

Fick's second law model was used to explain the active substance extraction process [27, 28]. To facilitate

Table 2 CPP extraction kinetic model

Model	Equation	Parameters	Reference
Second-order model	$C_t = \frac{C_s^2 kt}{1+C_s kt}$	C_s, k, and h	[20, 25, 26, 55]
Fick's second law model	$\ln[(\rho_{w\infty})/(\rho_{w\infty} - \rho_{w0})] = \mathrm{kt} + \ln b$	K and Ds	[27, 28, 56]
Peleg model	$C_t = \frac{t}{K_1+K_2 t}$	K_1 and K_2	[29, 45, 57]

subsequent research for CPP extraction, simplified assumptions were made for the extraction process:

(1) The pulverized particles of CP with different particle sizes are regarded as spherical, and the shape remains unchanged during the entire extraction process without solvent influence.
(2) Polysaccharides only diffuse with uniform concentration from the core to the outside along the direction of their particle size.
(3) The mass transfer resistance of polysaccharides on the surface of CP particles is negligible.
(4) When the solute diffuses into the solvent, the extraction time, temperature, solid–liquid ratio, and particle size have no effect on the concentration of each point in the solvent, and the uniform diffusion coefficient of each point of the main mass concentration of the liquid phase remains unchanged.
(5) CP particles are evenly distributed in the solvent, and the external solution is a uniform field, and the temperature is consistent with the solvent.

According to Fick's second law of diffusion:

$$\frac{\partial \rho_C}{\partial \mathrm{t}} = D_\tau \left(\frac{\partial^2 \rho_C}{\partial^2 \mathrm{x}} + \frac{\partial^2 \rho_C}{\partial^2 \mathrm{y}} + \frac{\partial^2 \rho_C}{\partial^2 \mathrm{z}} \right) \tag{6}$$

where $\frac{\partial^2 \rho_C}{\partial^2 \mathrm{x}}, \frac{\partial^2 \rho_C}{\partial^2 \mathrm{y}}, \frac{\partial^2 \rho_C}{\partial^2 \mathrm{z}}$, is the mass concentration gradient on the *x*-, *y*-, and *z*-axis . $\frac{\partial \rho_C}{\partial \mathrm{t}}$ is the mass concentration–time gradient.

Assumption $\Delta \rho_c = \frac{\partial^2 \rho_C}{\partial^2 \mathrm{x}} + \frac{\partial^2 \rho_C}{\partial^2 \mathrm{y}} + \frac{\partial^2 \rho_C}{\partial^2 \mathrm{z}}$, due to the above assumption that the grains of CP are assumed to be spherical, the following Eq. (7) was obtained.

$$\Delta^2 \rho_c = \frac{\partial^2 \rho_C}{\partial r^2} + \frac{\partial \rho_C}{\partial \mathrm{r}} \cdot \left(\frac{2}{r} \right) \tag{7}$$

If $\mathrm{f} = \rho_c \bullet r$, then Eq. (8) was expressed as follows.

$$\frac{\partial f}{\partial t} = D_\tau \cdot \frac{\partial^2 f}{\partial r^2} \tag{8}$$

Assuming boundary conditions $r = 0$, $f = 0$, $r = R$, Eq. (9) was given as follows.

$$\left(\frac{\partial \rho_W}{\partial \mathrm{t}} \right) \cdot \mathrm{V} = -D_\tau S \left(\frac{\partial \rho_C}{\partial \mathrm{r}} \right)_{R=r} \tag{9}$$

Initial conditions $t = 0, f = \rho_{c0} r$; $t = \infty, \rho_{w\infty} = \rho_{c\infty}$. From the Fourier transform method, we can get Eq. (10).

$$\frac{\rho_{w\infty} - \rho_w}{\rho_{w\infty} - \rho_{w0}} = (6/\pi^2) \sum_{n=1}^{\infty} \left\{ \exp[-(n\pi/R)^2 D_\tau t] \right\} \tag{10}$$

Because the high-order term of the mass concentration distribution tends to 0, when $n = 1$, Eq. (11) was expressed.

$$\frac{\rho_{w\infty} - \rho_w}{\rho_{w\infty} - \rho_{w0}} = \left(\frac{6}{\pi^2} \right) \left[\exp\left(-\frac{\pi^2 D_\tau t}{R^2} \right) \right] \tag{11}$$

At the initial extraction time, $\rho_{w0} = 0$ is taken, and the logarithm on both sides of the logarithm (10) is obtained by Eq. (12).

$$\ln[(\rho_{w\infty})/(\rho_{w\infty} - \rho_{w0})] = \mathrm{kt} + \ln b) \tag{12}$$

where $k = \frac{\pi^2 D_\tau}{R^2}$, $b = \frac{\pi^2}{6} = 1.643$, t is the extraction time, min; R is the radius, mm; ρ_C is the mass concentration of the polysaccharides within the particle at the distance r from the surface of the sphere at time t, mg/mL;D_τ is the surface diffusion coefficient; ρ_w is the mass concentration of the polysaccharides in the main body of the liquid phase at time t, mg/mL; V is the volume of the solvent in the main body of the liquid phase, mL; S is the contact area between the material particles and the solvent, mm^2; ρ_{c0} is the initial mass concentration of the solute in the particles, mg/mL; ρ_{w0} is the initial mass concentration of the solute in the main body of the liquid phase, mg/mL; $\rho_{c\infty}$ is the initial mass concentration of the solute in the granule at the extraction equilibrium, mg/mL; and $\rho_{w\infty}$ is the mass concentration of the solution at the equilibrium extraction, mg/mL. Equations (7) and (8) are the obtained kinetic equations, which are used to reflect the relationship among the radius of the CP, the extraction time, the temperature, the liquid to material ratio, and the polysaccharide mass concentration.

2.3.3 Peleg model

The Peleg model was applied to the prediction of CPP extraction behavior. This model has been used in experiments such as polyphenols and volatile oil extraction [29]. Therefore, the Peleg model was tried to study the extraction of CPP. Equation (13) describing the model is displayed as follows:

$$C_t = \frac{t}{K_1 + K_2 t} \tag{13}$$

$$\frac{t}{C_t} = K_1 + K_2 t \tag{14}$$

In the Peleg model, C_t is the polysaccharide concentration at time t (mg/mL), and K_1 is the Peleg ratio constant (g polysaccharide/100 g dry matter), which is related to the B_0 extraction rate (g polysaccharide/100 g dry matter, min) at the beginning of the extraction ($t = 0$), as shown in Eq. (14):

$$B_0 = \frac{1}{K_1} \tag{15}$$

The Peleg capacity constant (K_2) is related to the maximum extraction yield and C_{sp} (g polysaccharide/100 g dry matter) is the extraction capacity of the Peleg model in equilibrium, defined in equation:

$$C_{sp} = \frac{1}{K_2} \tag{16}$$

2.4 Physical and chemical properties

Chemical composition of CPP was determined by classical methods provided in the literature, including the polysaccharide content determination [24], the protein content measure [30], the content of uronic acid analysis [31], and the content of sulfate group determination [32]. Each experiment was repeated three times and the average value was obtained.

2.5 Rheology analysis of CPP

The freeze-dried CPP was dissolved in distilled water, and the effects of treatment time, concentration, pH, ionic strength, temperature, additional amount (K^+, Zn^+, Na^+, and Ca^{2+}), and salt on the viscosity of polysaccharides were studied, respectively, and the data was recorded using a digital viscometer in continuous reading mode (SNB-2, Shanghai Tianmei Tianping Instrument Co., Ltd., China). Each group of experiments was repeated three times and the average value was taken.

2.5.1 The effect of heat treatment temperature on CP viscosity

We took the same volume of CPP solution (5%) into four beakers, followed by stirring for 30 min at a constant temperature of 40, 60, 80, and 100 °C for 1 h, respectively. The viscosity of CPP was measured at 20 °C [33–35].

2.5.2 The effect of heat treatment time on the viscosity of CPP

A 5% CPP solution with the same volume was prepared in five beakers, heated at 80 °C, and then stirred for 20, 30, 40, 50, and 60 min, respectively. When the temperature declined at 20 °C, the viscosity of CPP was measured [33–35].

2.5.3 The effect of pH on the viscosity of CPP

The same volume of 5% CPP solution was added into five beakers, and the solution pH was adjusted to 2, 4, 6, 8, and 10 using NaOH (1 mol/L) or HCl (1 mol/L), respectively. After stirring for 1 h, the viscosity of CPP was measured at 20 °C [33–35].

2.5.4 The effect of different concentrations of sucrose, NaOH, antioxidant Vc, and oxidant H_2O_2 on the viscosity of CPP

Sucrose, NaOH, antioxidant Vc, and oxidant H_2O_2 were added into the 5% CPP solution to a final concentration of 0.5%, 2.5%, 5%, and 10%, respectively. Then, the viscosity of solution was determined after keeping 1 h at 20 °C [33–35].

2.5.5 The effect of metal ions on the viscosity of CPP

Different concentrations of NaCl, KCl, $CaCl_2$, and MgCl solutions were added into the 5% CPP solution. Then, the viscosity of the solution was determined after keeping 1 h at 20 °C [33–35].

2.5.6 The viscosity of different concentration CPP determination

CPP was dissolved in distilled water and stirred slowly at room temperature to prepare a crude polysaccharide solution with a concentration of 0.05 mg/mL, 0.1 mg/mL, and 0.2 mg/mL. Then, the prepared polysaccharide solution was stored at 4 °C for 5 h to make it completely hydrated. We kept each sample in a water bath at 25 °C for 10 min before the test, and then the apparent viscosity of different concentration CPP was measured with a digital viscometer [33] (SNB-2, Shanghai Tianmei balance instrument Co., Ltd., Shanghai, China).

2.6 Determination of α-amylase and α-glucosidase inhibitory activities in vitro

The α-amylase activity inhibition experiment was slightly modified according to the method from the literature [36–38]. CPP was dissolved in 0.2 mol/mL PBS (pH = 6.6) to prepare polysaccharide solutions of 1, 2, 3, 4, 5, and 6 mg/mL, respectively. 0.25-mL sample solutions of different concentrations were added to 0.25 mL α-amylase solution (6 U/mL, Solarbio Biotechnology Co., Ltd.) and 0.5 mL PBS at 37 °C for 10 min, respectively. Then, 0.5 mL 1% soluble starch solution and 1 mL DNS reagent were added into the above mixture solution for reacting at 37 °C for 5 min. The reaction solution was cooled rapidly in an ice water bath, and placed in a boiling water bath. After diluted with 5 mL

distilled water, the absorbance was determined at 540 nm. At the same time, the sample control group was made. Each experiment was repeated three times; the α-amylase inhibition rate was calculated with formula (17):

$$\alpha-\text{amylaseinhibitionrate}(\%)=\left[1-\frac{\left(A_3-A_4\right)}{\left(A_1-A_1\right)}\right]*100 \tag{17}$$

where A_1 is the absorbance of the blank tube, A_2 is the absorbance of the blank control tube, A_3 is the absorbance of the suppression tube, and A_4 is the absorbance of the suppression control tube.

The inhibitory effect of CPP on α-glucosidase was evaluated with p-NPG (Solarbio Biotechnology Co., Ltd.) as a substrate. The above different concentrations of CPP solution were mixed with 10 µL α-glucosidase solution (1U) (Solarbio Biotechnology Co., Ltd.), and 50 µL phosphate buffer solution 100 mM (pH 6.8) at 37 °C for 15 min. Then, 20 µL 5 mM · P-NPG was added at 37 °C for 20 min, and then 50 µL 0.1 M Na_2CO_3 solution was added to terminate the reaction. Acarbose solution was used as the standard [36–38], and the absorbance was measured under 405 nm, and the sample was used as control. Each experiment was repeated 3 times, and the inhibition rate was calculated with formula (18):

$$\alpha-\text{glycosidaseinhibitionrate}(\%)=\left[1-\frac{B_1-B_2}{B_3-B_4}\right]*100 \tag{18}$$

where B_1 is sample group absorbance, B_2 denotes sample blank group absorbance, B_3 represents control group absorbance, and B_4 shows control blank group absorbance.

2.7 Structural characterization of CPP

2.7.1 Scanning electron microscopy (SEM)

The CPP samples were placed on the viscous sample table and placed on the gold-plated conductive layer in the vacuum spray plating instrument. The samples were observed by a scanning electron microscope and photographed by self-contained software (JSM-5600L V, American Kevex Company, America) [39].

2.7.2 Differential thermal analysis and thermogravimetric analysis (DTA/TG)

The DTA/TG curve of 2.0 mg CPP was used to analyze the thermal characteristics of CPP [40, 41] using a thermogravimeter (STA449C, Netzsch, Germany) at a temperature from 25 to 900 °C with a heating rate of 10 °C/min.

2.7.3 Fourier infrared (FT-IR) spectroscopy analysis

Two milligrams of CPP was mixed with 300 mg KBr powder in a small mortar and ground evenly. The CPP was pressed into a thin sheet by a pressing machine, and the infrared spectrum was scanned on the wave number 400–4000 cm^{-1} by an infrared spectrometer (Nexus 670 FT-IR, USA) [27]. Each sample was scanned three times.

2.7.4 Atomic force microscopy (AFM) observation

Mica film was used as the negative film of AFM (Multi-Mode-HR, Brooke, USA). The concentration of 1.0 µg/mL CPP aqueous solution was prepared at room temperature overnight. The sample solution was dripped on the newly stripped mica surface by a traditional drip deposition method, and then dried naturally and tested under AFM. The morphological features of AFM images (such as height, width) were analyzed by the software attached to the atomic force microscope [42].

2.8 Data analysis

All the experiments were repeated three times. The experimental results were analyzed by Origin Pro software (version 8.0, Stat-Ease Inc. Minneapolis, MN, USA). Analysis of variance by Tukey's test ($p<0.05$) (ANOVA) evaluates the significant difference by SPSS software (version 21.0, SPSS Inc, Chicago, IL, USA).

3 Results and discussion

3.1 Extraction kinetics

3.1.1 Effect of extraction temperature on the yield of CPP

Generally, the two phenomena of thermal effect and cavitation effect play an important role. The thermal effect works by expanding and loosening the cell structure, while the cavitation effect works by imposing cavitation bubbles or holes [27, 43, 44]. Temperature is the most important parameter during the polysaccharide extraction process, because many factors (such as viscosity, diffusion coefficient, and solubility) are related to the temperature of the extraction solvent. The extraction efficiency increases with the increasing temperature. The effect of temperature on the extraction process was attributed to the diffusivity and solubility of biomass [43–46]. At higher temperatures, the solvent with the higher solvent vapor pressure fills the cavitation bubbles, and the cavitation bubbles collapse with low strength, resulting in reduced cavitation [36, 47].

The temperature slowly rose in the initial stage (40 ~ 60 °C), and the diffusion and mass transfer of CPP significantly increased due to an acceleration of molecular motion (Fig. 1A). In this stage, the higher concentration of CPP could be obtained because the higher temperatures could decrease the dielectric constant and polarity of water (in turn due to the decrease in the polar force between water molecules). Besides, as the solve temperature increases, the viscosity of the solve decreased, and the surface tension and diffusion coefficient of the solve increased, resulting in an increase in the mass transfer rate of the solute from the sample matrix to the solvent. In the diffusion stage, the growth rate of CPP yield was small; with the increase of temperature (70 ~ 80 °C), the CPP concentration increased very slowly. The phenomenon implied that the extraction process has arrived at phase balance. The increase of temperature is beneficial for the solvent to enter into the interior and increase the solubility of CPP in the solvent. The maximal yield of polysaccharides was obtained at 15.56%, while extraction temperature 80 °C, material-liquid ratio 1:16, extraction time 80 min, and particle size 180 μm.

3.1.2 Effect of solid–liquid ratio on the yield of CPP

In the presence of sufficient biomass to solvent ratio, due to the large concentration difference between the biomass matrix and the solvent system, a better mass transfer from the particle surface to the solvent can be achieved [48–50]. With the increase of solid–liquid ratio, the contact area between CP particles and solvents increased, the concentration gradient of polysaccharides increased gradually in the boundary of inside and outside CP particles, and the mass transfer driving force increased to promote mass transfer and diffusion, thus achieving the purpose of strengthening the CPP extraction and increasing the diffusion rate.

The yield of CPP increased with the increase of solid–liquid ratio, but the concentration of CPP decreased slowly due to the increase of solvent volume. When the ratio of material to liquid reached at 1:16, extraction time was set as 80 min, the extraction temperature was 80 °C, and the particle size is 180 μm, the maximum CPP yield was 15.56% (Fig. 1A).

3.1.3 Effect of particle size on the yield of CPP

The particle size played an important role in increasing the yield during the extraction process [29]. By reducing the particle size, the surface area of the material in contact with the solvent is increased, and the mass transfer rate was also increased, and a higher yield can be obtained in a short extraction time [45, 51]. In the case of large particle size, percolation of solvent during extraction was slow due to the large pore length, i.e., higher diffusion resistance and a lower specific surface area per unit mass [44, 52]. The finer particles lead to enhance mass transfer due to the deep penetration of the solvent and the larger surface area (providing high surface contact between the particles and the solvent). The reduction of particle size will help to increase the concentration of CPP in the solvent (Fig. 1B). The rapid increase of CPP yield was observed when the particle size decreased from 420 to 180 μm, and the optimal particle size is 180 μm; the maximum CPP yield was 15.56%.

3.1.4 Effect of extraction time on the yield of CPP

Under different extraction condition combinations, the yield of CPP increased significantly with the increase of extraction time (Fig. 1B). The reason could be attributed to that with the extension of the extraction time, CPP was dissolved by the extraction solvent, and then diffused from the CP particles interior to the surrounding solvent. As the extraction time was further extended, the CPP concentration inside and outside the particles tended to balance, and the concentration in the extract solve had reached saturation. Therefore, the CPP concentration change remained minor during the late extraction stage. The extraction rate of polysaccharides was 5.58% less at 10 min than at 80 min. If the extraction time was extended when the equilibrium is reached, the polysaccharide may be hydrolyzed, so the extraction time should not be too long. Hence, the optimal extraction time was chosen as 80 min.

3.2 CPP extraction kinetic model

To clarify the best kinetic model of hot-water extraction of CPP, three models were selected to study the extraction behavior according to the experimental design shown in sTable 1; where the particle size was chosen as 420 μm, 250 μm, and 180 μm; the ratio of solid–liquid was set as 1:16; extraction temperature changed from 40 to 80 °C; extraction time changed from 10 to 80 min; and the concentration of CPP was measured under different extraction conditions, all data were used to established three kinetic models.

3.2.1 Peleg model

The Peleg model equation was generated by fitting the experimental data of different CPP extraction combinations. The fitting curve and four kinetic parameters (K_1, K_2, B_0, C_{sp}) were obtained, respectively (Table 3). We found all curve agreed well with the Peleg model; the R^2 value was ≥ 0.98. The value of K was inversely proportional to the concentration of CPP. When the particle size increased from 180 to 420 μm, K_1 increased significantly from 12.035 to 19.585. K_2 increased from 1.16 to 1.21 with the particle size increase from 180 to 250 nm; however, the value change remained minor with 1.21 when the particle size increases from 250 to 420 μm. The

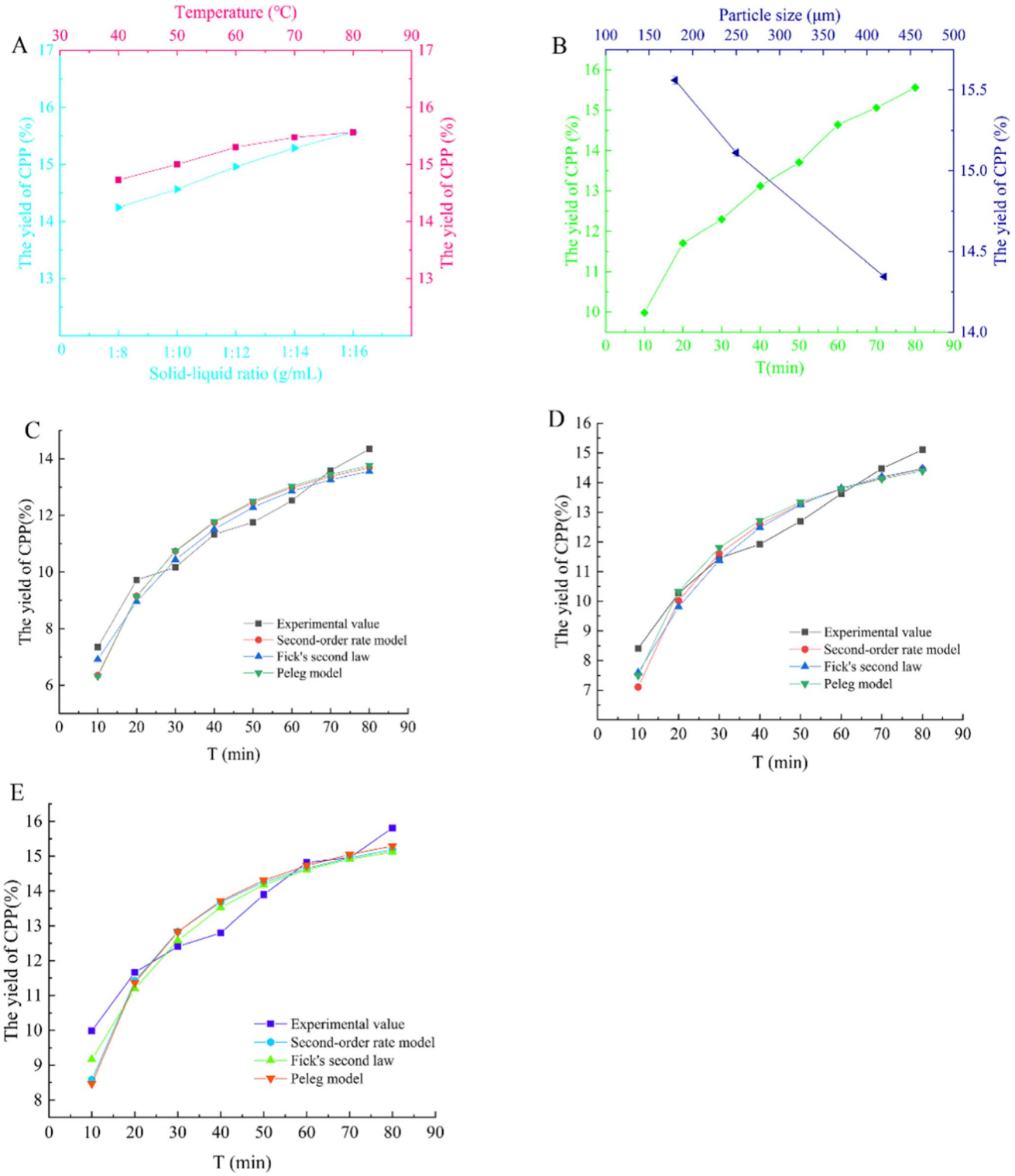

Fig. 1 The effect of different extraction factors on the yield of CPP. **A** The extraction yield curve (rose red) of CPP in different temperatures when the extraction time is 80 min, the ratio of material to liquid is 1:16, and the particle size is 180 μm. The extraction yield curve (baby blue) of CPP in different solid–liquid ratio when the extraction temperature is 80 °C, the extraction time is 80 min, and the particle size is 180 μm. **B** The extraction yield curve (green) of CPP in different time when the extraction temperature is 80 °C, the ratio of solid to liquid is 1:16, and the particle size is 180 μm. The extraction yield curve (dark blue) of CPP in different particle size when the extraction temperature is 80 °C, the ratio of solid to liquid is 1:16, and the extraction time is 80 min. The model prediction and experimental curve under different particle sizes (420 μm (**C**),150 μm (**D**), 280 μm (**E**))

Table 3 Related parameters of the Peleg model under various factors

Particle size (μm)	Temperature (°C)	Solid–liquid ratio (g/mL)	$\frac{t}{C} = K_1 + K_2 t$	R^2	K_1	K_2	B_0	C_{sp}
		8	Y = 1.1533x + 21.798	0.98	12.80	1.15	0.08	0.87
		10	Y = 1.2081x + 16.158	0.98	16.16	1.21	0.06	0.83
180	80	12	Y = 1.1478x + 18.43	0.98	18.43	1.15	0.05	0.87
		14	Y = 1.194x + 11.129	0.99	11.13	1.19	0.09	0.84
		16	Y = 1.1574x + 12.035	0.99	12.04	1.16	0.08	0.86
	40		Y = 1.422x + 18.856	0.98	18.86	1.42	0.05	0.70
	50		Y = 1.199x + 15.993	0.99	15.99	1.20	0.06	0.83
180	60	16	Y = 1.2069x + 10.989	0.99	10.99	1.21	0.09	0.83
	70		Y = 1.1455x + 14.037	0.99	14.04	1.15	0.07	0.87
	80		Y = 1.1574x + 12.035	0.99	12.04	1.16	0.08	0.86
420			Y = 1.2087x + 19.585	0.98	19.59	1.21	0.05	0.83
250	80	16	Y = 1.2076x + 14.598	0.99	14.60	1.21	0.07	0.83
180			Y = 1.1574x + 12.035	0.99	12.04	1.16	0.08	0.86

results indicated that the change of particle size had different degrees of influence on the kinetic parameters. K_1 was proportional to particle size, but the effect of particle size on K_2 was small, but the overall trend was increasing. B_0 and equilibrium concentration (C_{sp}) increased with the decrease of particle size, and the extraction rate is increasing. With the continuous increase of temperature and solid–liquid ratio, the two parameters (B_0 and C_{sp}) of the fitting equation did not change much, and there was no significant regularity.

When the Peleg model was applied to the experimental data of CPP extraction (Table 3), the overall fitting of the experimental data was good, but the applicability of the whole extraction process was poor, especially for the fitting effect of temperature and solid–liquid ratio. It cannot well describe the behavior of CPP extraction during the entire extraction period. It is necessary to explore better extraction models.

3.2.2 Second-order rate model

It can be seen from Fig. 1 that the CPP content increases significantly with the increase of extraction time at a different temperature, particle size, and ratio of material to liquid. The reason is that with the extension of extraction time, CPP was dissolved by the extraction solvent, and then diffuses from the CP particles to the surrounding solvent, thus increasing the content of CPP. The second-order rate model was used to fit the data. As shown in Table 4 below: $\frac{t}{C_t} = \frac{1}{h} + \frac{t}{C_S}$ has a good linear relationship ($R^2 > 0.98$) for plotting t. We determine the kinetic parameters (h, K, C_s) based on the regression of the second-order rate model in the saturated state. According to the data in Table 4, the second-order rate constant K reflects the extraction rate of the extraction process.

It can be found from Eq. (4) that the K value is located in the denominator in the second-order model fitting curve,

Table 4 Related parameters of the second-order rate model under various factors

Particle size (μm)	Temperature (°C)	Solid–liquid ratio (g/mL)	$\frac{t}{C_t} = \frac{1}{h} + \frac{t}{C_S}$	R^2	h	C_s	K
		8	Y = 1.2199x + 18.199	0.99	0.05	0.82	27.08
		10	Y = 1.2454x + 14.932	0.99	0.07	0.80	23.16
180	80	12	Y = 1.1634x + 17.929	0.98	0.06	0.86	24.27
		14	Y = 1.1945x + 10.963	0.99	0.09	0.84	15.64
		16	Y = 1.1724x + 11.572	0.99	0.09	0.85	15.91
	40		Y = 1.1922x + 17.821	0.99	0.06	0.84	25.33
	50		Y = 1.1739x + 16.967	0.99	0.06	0.85	23.38
180	60	16	Y = 1.1748x + 13.546	0.99	0.07	0.85	18.70
	70		Y = 1.1707x + 12.745	0.99	0.08	0.85	17.47
	80		Y = 1.1724x + 11.572	0.99	0.09	0.85	15.91
420			Y = 1.22x + 19.304	0.98	0.05	0.82	28.73
250	80	16	Y = 1.1693x + 16.349	0.99	0.06	0.86	22.35
180			Y = 1.1724x + 11.572	0.99	0.09	0.85	15.91

and the smaller the K value, the faster the solute diffuses from the CP particles to the solvent. Similar to the Peleg model, the particle size is proportional to the rate constant and inversely proportional to the saturation concentration. When the solution is saturated, the difference between the maximum concentration and the minimum concentration is 0.03, and the difference of K value is 12.82 (between 180 ~ 420 μm). Under the influence of temperature, material-liquid ratio, and other factors, although the overall rate constant is decreasing and the saturation concentration is increasing, there is no obvious regularity. It may be due to the poor fit between the experimental value and the second-order rate model, resulting in a large deviation. Although the fitting curve has a good linear relationship, the second-order rate model has a poor fit and cannot fully reflect the entire extraction process of CPP, so it is necessary to explore a better extraction model.

3.2.3 Fick's second law

The ln $[\rho w_{\infty} / (\rho w_{\infty}\text{-}\rho_{w})]$ has a good linear relationship for the mapping of time t ($R^2 > 0.89$) (Table 5), so the CPP extraction is in accord with the first-order kinetic model. The slope of each curve was the rate constant k, which could reflect the speed of polysaccharide extraction. With the increase of liquid-material ratio and temperature, the particle size decreased and the rate constant k gradually increased, indicating that the extraction rate of polysaccharides in the extract increased, so the change of these conditions was beneficial to the extraction of CPP. It could be seen from Table 5 that $D\tau$ also increases with the increase of extraction temperature and solid–liquid ratio, and decrease of particle size. The driving force of polysaccharide extraction is the mass concentration difference, the concentration difference increases with the increase of solvent, the movement of polysaccharide molecules increases with the increase of temperature, and the particle size makes the solute quickly from raw material to solvent, which will increase the calculated $D\tau$ relatively. Based on Fick's second law, a CPP extraction kinetic model was established, and the key kinetic parameters such as the rate constant and diffusion coefficient under different temperatures, material to liquid ratio, particle size, and time were obtained. The results show that the experimental data was in good agreement with the calculated value of the kinetic model, and the extraction rate fitting curve is divided into two stages: a fast-rising trend and a slow rising to equilibrium. The whole extraction process was relatively easy to carry out. It could provide a valuable theoretical basis for the design of the CPP production process and the selection and optimization of operating conditions.

3.3 CPP physical and chemical properties test results

The dried CPP was white, odorless, and powdery, and has good thermal stability. The content of the sulfate group in CPP was 3.13% determined by barium sulfate turbidity. The content of galacturonic acid determined by the sulfuric acid-carbazole method was 4.03%. The results of the BCA method showed that the protein content in CPP was 0.25%.

3.4 Rheological properties of CPP

3.4.1 The effect of heat treatment temperature on the viscosity of CPP

The increasing temperature strengthened the thermal movement of molecules and weakened the cross-linking and aggregation between molecules. The flexibility of molecular chains was enhanced; the fluidity of CPP solution increased.

Table 5 Related parameters of Fick's second law under various factors

Particle size (μm)	Temperature (°C)	Solid–liquid ratio (g/mL)	$\ln[(\rho_{w\infty})/(\rho_{w\infty} - \rho_{w0})] = k\tau + \ln b$	R^2	K	$D\tau$
		8	Y = 0.0334x + 0.3455	0.94	0.033	0.36
		10	Y = 0.0341x + 0.3504	0.94	0.034	0.37
180	80	12	Y = 0.036x + 0.463	0.96	0.036	0.39
		14	Y = 0.0362x + 0.3455	0.95	0.036	0.39
		16	Y = 0.0382x + 0.5075	0.95	0.038	0.41
	40		Y = 0.0352x + 0.336	0.99	0.035	0.38
	50		Y = 0.0327x + 0.4771	0.89	0.036	0.39
180	60	16	Y = 0.0336x + 0.2582	0.91	0.037	0.39
	70		Y = 0.0394x + 0.554	0.99	0.039	0.42
	80		Y = 0.0382x + 0.5075	0.97	0.038	0.41
420			Y = 0.0321x + 0337	0.92	0.032	0.35
250	80	16	Y = 0.035x + 03,474	0.93	0.035	0.38
180			Y = 0.0382x + 0.5075	0.97	0.038	0.41

As shown in Fig. 2A, the viscosity of CPP decreases rapidly with increasing temperature from 40 to 100 °C. The viscosity of CPP aqueous solution was 0.444 Pa·s at 40 °C, and when the temperature was raised to 100 °C, the viscosity decreased at 0.083 Pa·s. The results could be explained that the higher temperature led to dehydration between polymer molecules in polysaccharides [14], the degree of polymerization and cross-linking was weakened, and the viscosity also was reduced.

3.4.2 The effect of pH on the viscosity of CPP

As shown in Fig. 2A, the change of pH value had a great influence on the rheological properties of the CPP solution. The viscosity of CPP solution increased gradually with the increase of pH from 2.0 to 6.0, and reached the maximum value of 0.24 Pa·s. With the increase of pH from 6.0 to 10.0, the solution viscosity decreased sharply to 0.093 Pa·s at pH 10.0. CPP was an acidic polysaccharide; the polysaccharide stretches the molecules through intermolecular repulsion and disperses in water to form a more stable conformation at around pH 5.0. At very low pH values, the higher concentrations of H^+ can inhibit the ionization of carboxyl groups in galacturonic acid of CPP, weaken the intermolecular electrostatic interaction, and degrade polysaccharide macromolecules under strong acid conditions. Hence, CPP has lower viscosity at very low pH. In a strongly alkaline environment with higher pH, OH^- can undergo acetylation and methyl esterification reactions with the methoxy group of polysaccharide molecules, which could shorten the molecular chain of polysaccharides, reduce the molecular weight, and decrease the viscosity of polysaccharides [53].

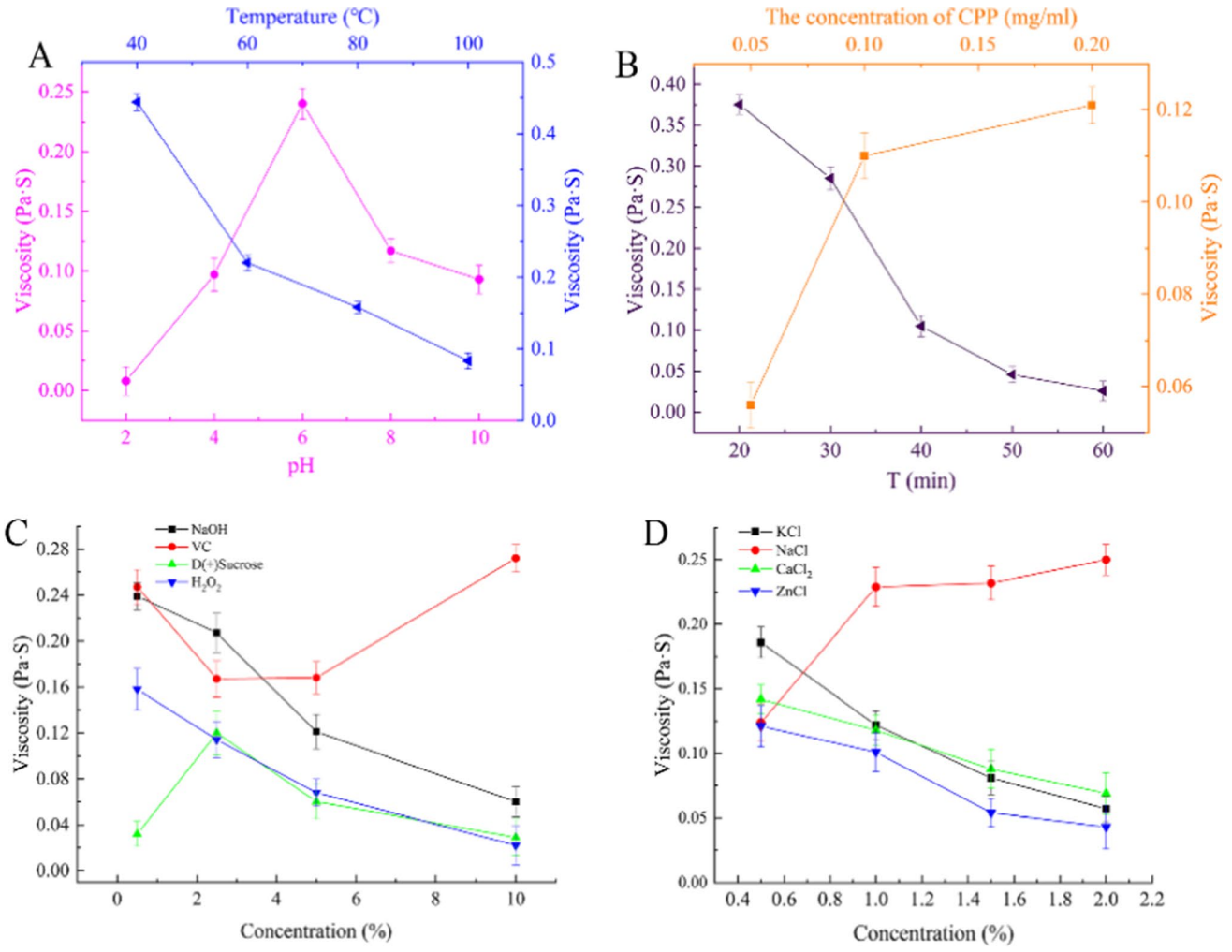

Fig. 2 Rheological properties of CPP under different treatment conditions. **A** The effect of different temperature and pH on the rheology of CPP. **B** The effect of different CPP concentration and test time on the rheology of CPP. **C** The effect of different concentrations of NaOH, Vc, and H_2O_2 on the rheology of CPP. **D** The effect of different concentrations of metal ions on the rheology of CPP

3.4.3 The effect of polysaccharide concentration on the viscosity of CPP

The viscosity of the CPP solution increased with the increase of CPP concentration shown in Fig. 2B. When the concentration range of CPP solution was 0.05 ~ 0.1 mg/mL, the viscosity of CPP increases the fastest from 0.056 to 0.11 Pa·s. When the concentration increased to 0.2 mg/mL, the viscosity increased to 0.121 Pa·s. CPP was a hydrophilic polymer with a chain-like linear conformation in aqueous solution. The number of polysaccharide molecules increased along with the increase of CPP concentration, the intermolecular hydrogen bonding and hydrophobic interaction forces increased, and the fluid flow resistance increased. Hence, polysaccharide solution viscosity gradually increased.

3.4.4 The effect of heat treatment time on the viscosity of CPP

As shown in Fig. 2B, the viscosity of CPP decreased rapidly with the prolongation of heating time at 80 °C. After heating from 20 to 30 min, the viscosity of CPP decreased by 24% from 0.375 to 0.285 Pa·s. When kept for 40 min, 50 min, and 60 min, the viscosity was 0.105 Pa·s, 0.046 Pa·s, and 0.026 Pa·s, respectively, and the viscosity decreased by 93.07%. In the early stage of heating, the viscosity decreased rapidly, which was mainly due to the chain breaking of polysaccharides at high temperature, the linear structure of a molecular chain and intermolecular cross-linking structure was gradually destroyed, and the degree of molecular polymerization was reduced, the increase of intermolecular dispersion made CPP solution viscosity rapidly decrease. The thermal effect on the structure of the CPP reached the maximum at 50 min. With the increase of the heat treatment time, the thermal effect on the molecular structure and molecular chain of the polysaccharides was not obvious, so the decreasing trend of viscosity became slow.

3.4.5 The effect of the concentration of sucrose, NaOH, Vc, and H_2O_2 on the viscosity of CPP

As shown in Fig. 2C, the viscosity of CPP solution increased slightly from 0.032 to 0.12 Pa·s with the addition of sucrose from 0.5 to 2.5%. The results showed that sucrose molecule containing hydroxyl groups can produce a synergistic thickening effect with CPP, which may form a new reticular structure through a hydrogen bond in an aqueous solution and lead to the viscosity increasing. Finally, the sucrose content continued to increase, the viscosity of CPP gradually decreased, and the concentration of CPP was 0.029 Pa·s when the addition of sucrose was 10%. It can be seen from Fig. 2C that the viscosity of CPP decreased with the increase of the amount of NaOH, indicating that CPP was unstable to alkali. The addition of H_2O_2 had a significant effect on the viscosity of CPP, and the viscosity decreased linearly with the increase of the amount of H_2O_2 (displayed in Fig. 2C). H_2O_2 is a strong oxidant, which could oxidize the hydroxyl groups of CPP and break the molecular chain of polysaccharides, resulting in the viscosity decrease. The effect of different concentrations of Vc on the rheology of CPP also can be seen from Fig. 2C; the viscosity was the smallest at the additive amount of 2.5%. However, when the addition of Vc was more than 5%, the viscosity increased gradually with the increase of the addition. This may be that the higher concentration Vc will intensify the intermolecular interaction of polysaccharides, thus increase the viscosity.

3.4.6 The effect of metal ions on the viscosity of CPP

The effects of different concentrations of K^+, Zn^+, and Ca^{2+} on the viscosity of CPP solution are exhibited in Fig. 2D; the viscosity of the CPP solution decreases along with the additive concentration increase. The concentration of K^+, Zn^+, and Ca^{2+} increased from 0.5 to 2%, and the solution viscosity decreased by 0.129, 0.073, and 0.078 Pa·s, respectively. Under the same ion concentration, the viscosity of the CPP solution decreased with the increase of K^+, Zn^+, and Ca^{2+} ionic strength. But the viscosity increases with the increase of Na^+ intensity, and the viscosity of CPP solution increases to the maximum 0.250 Pa·s at 2%. We believed that the strong electrostatic interaction caused by the addition of K^+, Zn^+, and Ca^{2+} may lead to the shrinkage of CPP molecule, and further reduced the apparent viscosity. In the presence of Na^+, the polysaccharide solution can maintain obvious pseudoplastic fluid characteristics [53].

3.5 Hypoglycemic activity

CPP exhibited a certain inhibitory activity on α-amylase (Fig. 3A). The inhibitory rate firstly increased and then decreased minorly with the increasing concentration. The inhibition rate increased rapidly and reached 10.72 ± 0.79% at 2.0 mg/mL CPP and reached the maximum of 25.82 ± 1.12% at 8.0 mg/mL. When the concentration increased to 10 mg/mL, the inhibition rate was 24.50 ± 0.33%.

As shown in Fig. 3B, CPP also displayed better inhibitory activity on α-glycosidase. The inhibition rate increased rapidly to 60.22 ± 1.26% at the concentration of 4.0 mg/mL, and then increased gradually to the maximum of 70.8 ± 1.43% at 10 mg/mL.

3.6 SEM observation

SEM could be carried out to observe the surface three-dimensional structure of polysaccharides [54]. By

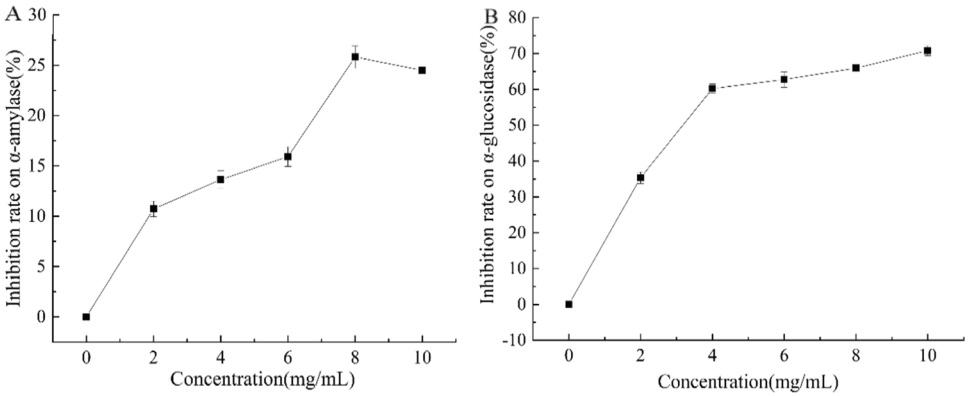

Fig. 3 Inhibition rate of different concentrations of CPP on α-amylase (**A**) and α-glycosidase (**B**)

adjusting the scanning observation multiple of SEM, the morphological characteristics of CPP were obtained in Fig. 4 with four magnification fields (×100, ×800, ×1000, and ×3000). It was found that CPP was a kind of loose irregular rod-shaped, rod-shaped, serrated, or honeycomb-like particle with a rough surface and more pore structure. The pore structure may form voids in the particles due to the drying process, causing some invagination to form more pores. Each rod-shaped, honeycomb-shaped, or zig-zag polysaccharide particle was composed of many dense small particles, and with the increase of magnification, the surface pores showed more obvious.

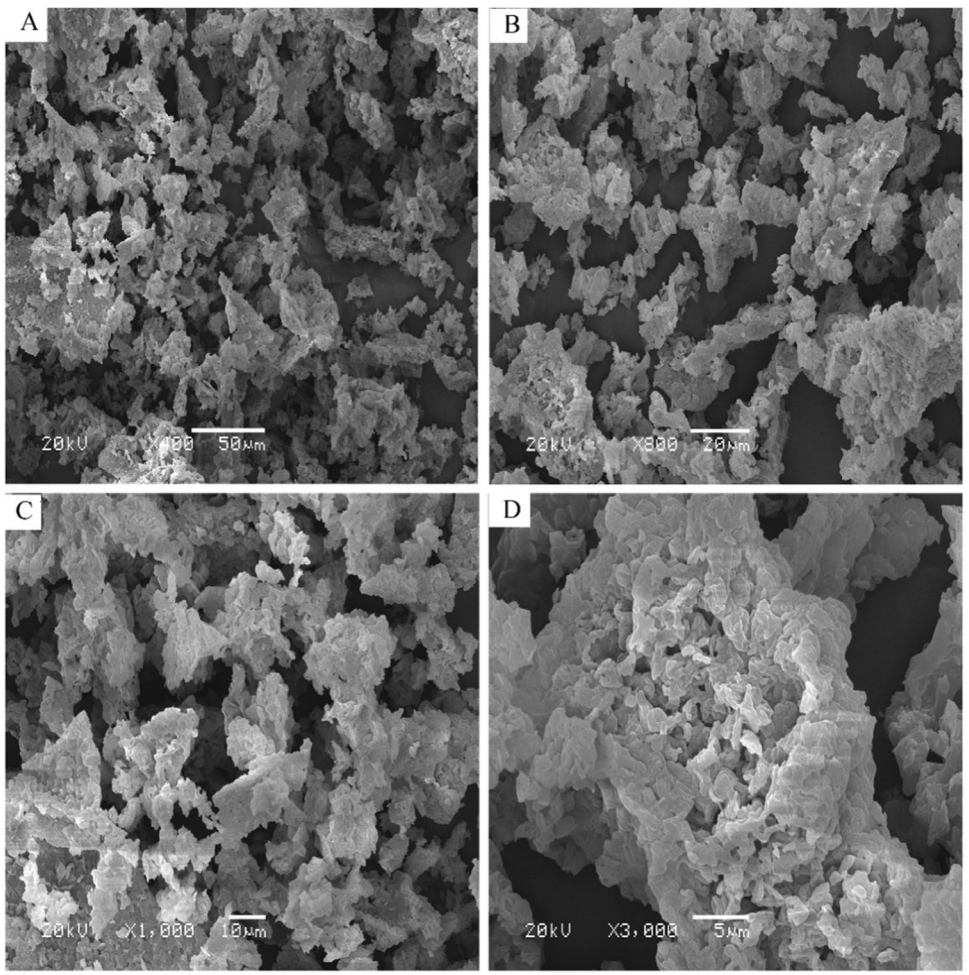

Fig. 4 Electron microscope pictures of CPP under different magnifications of ×100 (**A**), ×800 (**B**), ×1000 (**C**), and ×3000 (**D**) by SEM observation

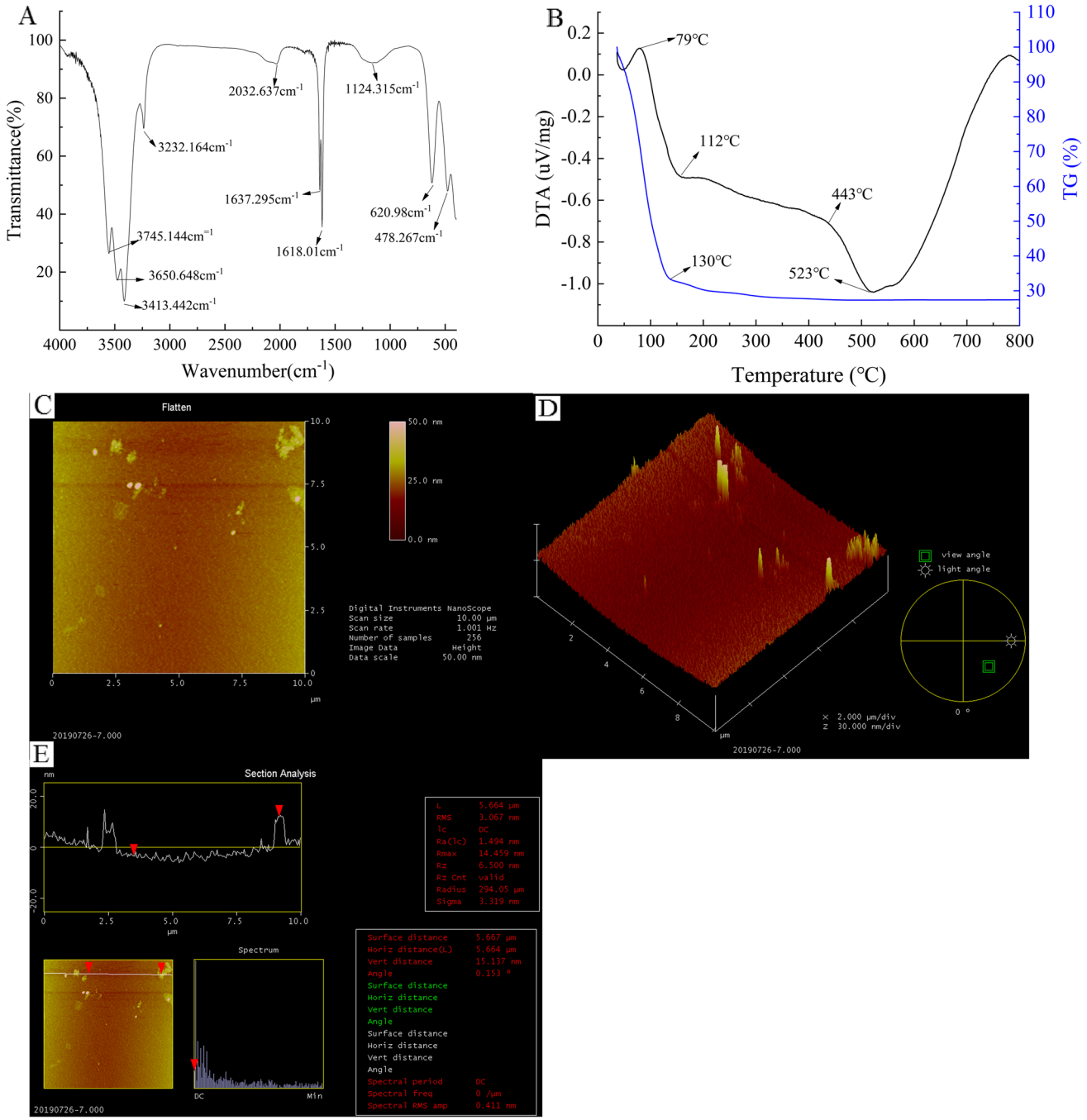

Fig. 5 Functional group structure characteristics of CPP by FT-IR (**A**), TG/DTA (**B**), and the microstructure characteristics of CPP were observed by AFM (**C**, **D**, **E**)

3.7 FT-IR analysis

The characteristic absorption peaks of CPP were analyzed by FT-IR and are shown in Fig. 5A. Some sharp peaks were found at 3745.144 cm^{-1} and 3650.648 cm^{-1}, which may be free -OH. The sharp peaks at 3413.44 cm^{-1} and 3232.164 cm^{-1} may be the stretching vibration of C-H on unsaturated carbon. The stretching vibration formed by the intramolecular association indicates that the polysaccharide has intermolecular and intramolecular hydrogen bonds. With the stretching vibration of the double bond at 2032.637 cm^{-1}, and the absorption peak and amido group of crystal water in the CPP at 1637.29 cm^{-1} C = O stretching vibration, it can be inferred that there may be -COOH in CPP, and there may be uronic acid in its composition. There were also many small impurity peaks on the curve, which

may be the interference of related reagents in the purification process of the extraction machine. The absorption peak of 1124.315 cm^{-1} indicated that the sugar ring configuration in CPP was pyran. The absorption peak of 620.98 cm^{-1} may be the vibration of a long carbon chain. 478.267 cm^{-1} may be the stretching vibration of a single bond or the bending vibration of a group, indicating that the monosaccharide residues of CPP may exist in the form of pyran rings.

3.8 Thermogravimetric and differential thermal analysis

The thermogravimetric curve of CPP showed the whole process can be divided into two stages (Fig. 5B). In the first stage, the sample quality decreased linearly from 0 to 130 °C. At this stage, the free water in the CPP was lost, and the weight loss rate reached 65.4%, indicating that CPP was decomposed in a large amount during this stage. Free water was adsorbed with weak force by van der Waals force [41]. This stage was accompanied by thermal decomposition of polysaccharides at 36.23 °C. The second stage was at 150–800 °C; the weight loss rate decreased slowly about 7.2% at this stage, indicating that CPP gradually decomposed completely. On the whole, the thermogravimetric range of CPP was mainly concentrated in 36.23 ~ 150 °C, and the total weight loss rate was about 72.6%. The quality loss in the second stage was due to carbonization and complete decomposition of intermediate products in this temperature range. At the beginning of the first stage, the rapid dehydration and decomposition of the glucose ring hydrocarbon group to form water molecules. In the second stage, the C–C-H, C = O, and C–C bonds were broken, and the main chain was also broken along with gas products CO, CO_2, and so on.

The DTA curve of CPP showed a strong endothermic peak (Fig. 5B) at 36 ~ 79 °C that could account for 27.1% of the total weight (corresponding weight loss on the TG curve). The endothermic reaction of dehydration, degassing, and softening plastic deformation occurred mainly at this stage. At 79 ~ 112 °C, the decomposition heat release of the DTA curve was accelerated, and the weight loss on the TG curve accounted for 31.9% of the total weight, which expressed combined water loss and oxidative decomposition. At 112 ~ 443 °C, the decomposition heat of the DTA curve slowed down, and the weight loss on the TG curve accounted for 13.7% of the total weight. As the temperature continued to rise, the weight of the sample did not change.

3.9 Atomic force microscopy

The density of the sugar chain is related to the initial mass concentration of the polysaccharide solution [42]. The higher concentration of polysaccharides with the large number of hydroxyl groups, the closer polymerization of polysaccharides chain maybe occurred, and the true morphology of polysaccharides cannot be observed. At the concentration of 1.0 μg/mL, the AFM images of CPP are shown in Fig. 5 (C, D, E). The density of branched chains per unit region was highlighted in Fig. 5 (C, D) that could explain the formation of polysaccharide aggregates with the increase of interchain action points and the enhancement of interchain forces under the action of hydrogen bonds and van der Waals forces. As shown in Fig. 5E, the CPP was on the mica sheet, the horizontal distance was 5.664 μm, the vertical distance was 15.13 nm, the surface distance was 5.667 μm, and the radius was 294.05 μm. In the case of overlapping complexes, the apex distance was 14.459 nm. The height of a polysaccharide molecule was 0.411 nm. Therefore, the size of the CPP molecule was within the theoretical value (0.1 ~ 1.0 nm) of the polysaccharide chain diameter.

4 Conclusion

In this study, three kinetic models of CPP extraction were established and comparative analysis. CPP extraction kinetics with hot water was more in line with Fick's second law model. The physical and chemical properties and microstructure of CPP also were determined. The highest CPP yield of 15.56% were obtained as extraction temperature 80 °C, material-liquid ratio 1:16, extraction time 80 min, and particle size 180 μm. The viscosity of CPP was inversely proportional to temperature, heating time, ion concentration (Ca^{2+}, K^+, Zn^+), sucrose, NaOH, and H_2O_2 content. However, the viscosity was proportional to the concentration of Vc and NaCl. CPP also had a significant inhibitory effect on α-glycosidase with more than 70% at 10.0 mg/mL.

Supplementary Information The online version contains supplementary material available at https://doi.org/10.1007/s13399-022-02518-w.

Author contribution Y G Wang and C L Wang contributed equally to this work. Y G Wang and F F Leng designed and revised the manuscript. C L Wang, M J Yang, H Y Xue, and Y M Jin performed the experiments and analyzed data. All authors have read and approved the manuscript.

Funding This study was financially supported by the National Natural Science Foundation of China (No. 31460032) and the Youth Talent Support Program of Lanzhou University of Technology (No. 2018).

Data availability All data that support the findings of this study are included within the article (and any supplementary files).

Declarations

Competing interests The authors declare no competing interests.

References

1. Xie M, Cheng J, Zhao G, Liu H, Zhang L, Yang C (2020) Natural wax from non-medicinal aerial part of Codonopsis pilosula as a biolubricant. J Cleaner Product 242
2. Ahmed T, Raza SH, Maryam A, Setzer WN, Braidy N, Nabavi SF, de Oliveira MR, Nabavi SM (2016) Ginsenoside Rb1 as a neuroprotective agent: a review. Brain Res Bull 125:30–43
3. Xu X, Yan H, Tang J, Chen J, Zhang X (2013) Polysaccharides in *Lentinus edodes*: isolation, structure, immunomodulating activity and future prospective. Crit Rev Food Sci Nutr 54(4):474–487
4. Zou Y-F, Zhang Y-Y, Paulsen BS, Fu Y-P, Huang C, Feng B, Li L-X, Chen X-F, Jia R-Y, Song X et al (2020) Prospects of *Codonopsis pilosula* polysaccharides: structural features and bioactivities diversity. Trends Food Sci Technol 103:1–11
5. Zou Y-F, Zhang Y-Y, Paulsen BS, Rise F, Chen Z-L, Jia R-Y, Li L-X, Song X, Feng B, Tang H-Q et al (2020) Structural features of pectic polysaccharides from stems of two species of *Radix Codonopsis* and their antioxidant activities. Int J Biol Macromol 159:704–713
6. Gao Z, Zhang C, Jing L, Feng M, Li R, Yang Y (2020) The structural characterization and immune modulation activitives comparison of *Codonopsis pilosula* polysaccharide (CPPS) and selenizing CPPS (sCPPS) on mouse in vitro and vivo. Int J Biol Macromol 160:814–822
7. Xin T, Zhang F, Jiang Q, Chen C, Huang D, Li Y, Shen W, Jin Y, Sui G (2012) The inhibitory effect of a polysaccharide from *Codonopsis pilosula* on tumor growth and metastasis in vitro. Int J Biol Macromol 51(5):788–793
8. Das D, Biswal S, Barhwal KK, Bhardwaj P, Kumar A, Hota SK, Chaurasia OP, Kumar B (2019) Methanolic root extract of *Codonopsis* clematidea prevents hypoxia induced procoagulant state by inhibition of GPIb receptor regulated Lyn kinase activation. Phytomedicine 59
9. Yin C, Noratto GD, Fan X, Chen Z, Yao F, Shi D, Gao H (2020) The impact of mushroom polysaccharides on gut microbiota and its beneficial effects to host: a review. Carbohydrate Polymers 250
10. Sun Q, Cheng L, Zeng X, Zhang X, Wu Z, Weng P (2020) The modulatory effect of plant polysaccharides on gut flora and the implication for neurodegenerative diseases from the perspective of the microbiota-gut-brain axis. Int J Biol Macromol 164:1484–1492
11. Liu C, Chen J, Li E, Fan Q, Wang D, Li P, Li X, Chen X, Qiu S, Gao Z et al (2015) The comparison of antioxidative and hepatoprotective activities of *Codonopsis pilosula* polysaccharide (CP) and sulfated CP. Int Immunopharmacol 24(2):299–305
12. Chen X, Han W, Wang G, Zhao X (2020) Application prospect of polysaccharides in the development of anti-novel coronavirus drugs and vaccines. Int J Biol Macromol 164:331–343
13. Zheng Z, Pan X, Xu J, Wu Z, Zhang Y, Wang K (2020) Advances in tracking of polysaccharides in vivo: labeling strategies, potential factors and applications based on pharmacokinetic characteristics. Int J Biol Macromol 163:1403–1420
14. Tao Y, Zhang Z, Sun DW (2014) Kinetic modeling of ultrasound-assisted extraction of phenolic compounds from grape marc: influence of acoustic energy density and temperature. Ultrason Sonochem 21(4):1461–1469
15. Piwowarska N, González-Alvarez J (2012) Extraction of antioxidants from forestry biomass: kinetics and optimization of extraction conditions. Biomass Bioenerg 43:42–51
16. Petigny L, Perino-Issartier S, Wajsman J, Chemat F (2013) Batch and continuous ultrasound assisted extraction of boldo leaves (Peumus boldus Mol.). Int J Mol Sci 14(3):5750–5764
17. Kim D-S, Lim S-B (2020) Kinetic study of subcritical water extraction of flavonoids from citrus unshiu peel. Separation Purif Technol 250
18. Ait Amer Meziane I, Bali N, Belblidia N-B, Abatzoglou N, Benyoussef E-H (2019) The first-order model in the simulation of essential oil extraction kinetics. J Appl Res Med Aromatic Plants 15
19. Cissé M, Bohuon P, Sambe F, Kane C, Sakho M, Dornier M (2012) Aqueous extraction of anthocyanins from Hibiscus sabdariffa: experimental kinetics and modeling. J Food Eng 109(1):16–21
20. Yedhu Krishnan R, Rajan KS (2016) Microwave assisted extraction of flavonoids from Terminalia bellerica: study of kinetics and thermodynamics. Sep Purif Technol 157:169–178
21. Alara OR, Abdurahman NH (2019) GC–MS and FTIR analyses of oils from Hibiscus sabdariffa, Stigma maydis and Chromolaena odorata leaf obtained from Malaysia: potential sources of fatty acids. Che Data Collect 20
22. Patil DM, Akamanchi KG (2017) Microwave assisted process intensification and kinetic modelling: extraction of camptothecin from *Nothapodytes nimmoniana* plant. Ind Crops Prod 98:60–67
23. Xiong Q, Huang S, Chen J, Wang B, He L, Zhang L, Li S, Wang J, Wu J, Lai X et al (2017) A novel green method for deproteinization of polysaccharide from *Cipangopaludina chinensis* by freeze-thaw treatment. J Clean Prod 142:3409–3418
24. Zhang WH, Wu J, Weng L, Zhang H, Zhang J, Wu A (2020) An improved phenol-sulfuric acid method for the determination of carbohydrates in the presence of persulfate. Carbohydr Polym 227:115332
25. Ha GS, Kim JH (2016) Kinetic and thermodynamic characteristics of ultrasound-assisted extraction for recovery of paclitaxel from biomass. Process Biochem 51(10):1664–1673
26. Patil DM, Akamanchi KG (2017) Ultrasound-assisted rapid extraction and kinetic modelling of influential factors: extraction of camptothecin from *Nothapodytes nimmoniana* plant. Ultrason Sonochem 37:582–591
27. Wang Y, Zhang X, Ma X, Zhang K, Li S, Wang X, Liu X, Liu J, Fan W, Li Y et al (2019) Study on the kinetic model, thermodynamic and physicochemical properties of Glycyrrhiza polysaccharide by ultrasonic assisted extraction. Ultrason Sonochem 51:249–257
28. Perez EE, Carelli AA, Crapiste GH (2011) Temperature-dependent diffusion coefficient of oil from different sunflower seeds during extraction with hexane. J Food Eng 105(1):180–185
29. Abugabr Elhag HEE, Ajit A, Sulaiman AZ (2020) Optimization and kinetic modelling of total water extracts and water soluble proteins in root extracts of *Eurycoma apiculata* by microwave assisted extraction. Materials Today: Proceedings 31:1–8
30. Cortes-Rios J, Zarate AM, Figueroa JD, Medina J, Fuentes-Lemus E, Rodriguez-Fernandez M, Aliaga M, Lopez-Alarcon C (2020) Protein quantification by bicinchoninic acid (BCA) assay follows complex kinetics and can be performed at short incubation times. Anal Biochem 608:113904
31. Filisetticozzi TMCC, Carpita NC (1991) Measurement of uronic acids without interference from neutral sugars. Anal Biochem 197(1):157–162
32. Tong H, Zheng X, Song J, Liu J, Ren T, Zhang X, Huang L, Wu M (2018) Radical scavenging activity of sulfated Bupleurum chinense polysaccharides and their effects against oxidative stress-induced senescence. Carbohydr Polym 192:143–149
33. Goh KK, Matia-Merino L, Chiang JH, Quek R, Soh SJ, Lentle RG (2016) The physico-chemical properties of chia seed polysaccharide and its microgel dispersion rheology. Carbohydr Polym 149:297–307

34. Shao P, Qin M, Han L, Sun P (2014) Rheology and characteristics of sulfated polysaccharides from chlorophytan seaweeds Ulva fasciata. Carbohydr Polym 113:365–372
35. Chen G, Chen K, Zhang R, Chen X, Hu P, Kan J (2018) Polysaccharides from bamboo shoots processing by-products: new insight into extraction and characterization. Food Chem 245:1113–1123
36. Huang Q, Chen S, Chen H, Wang Y, Wang Y, Hochstetter D, Xu P (2013) Studies on the bioactivity of aqueous extract of pu-erh tea and its fractions: in vitro antioxidant activity and alpha-glycosidase inhibitory property, and their effect on postprandial hyperglycemia in diabetic mice. Food Chem Toxicol 53:75–83
37. Djeridane A, Hamdi A, Bensania W, Cheifa K, Lakhdari I, Yousfi M (2015) The in vitro evaluation of antioxidative activity, alpha-glucosidase and alpha-amylase enzyme inhibitory of natural phenolic extracts. Diabetes Metab Syndr 9(4):324–331
38. Kasipandi M, Manikandan A, Sreeja PS, Suman T, Saikumar S, Dhivya S, Parimelazhagan T (2019) Effects of in vitro simulated gastrointestinal digestion on the antioxidant, α-glucosidase and α-amylase inhibitory activities of water-soluble polysaccharides from Opilia amentacea roxb fruit. Lwt 111:774–781
39. Boufi S, Bel Haaj S, Magnin A, Pignon F, Impéror-Clerc M, Mortha G (2018) Ultrasonic assisted production of starch nanoparticles: structural characterization and mechanism of disintegration. Ultrason Sonochem 41:327–336
40. Vardhanabhuti B, Ikeda S (2006) Isolation and characterization of hydrocolloids from monoi (*Cissampelos pareira*) leaves. Food Hydrocolloids 20(6):885–891
41. Zhang YF, Liu ZK, Lin YC, Liu PF (2019) Monosaccharide composition, thermogravimetric and thermal gravimetric analysis of Corlex Periplocae polysaccharide. Science and Technology of Food Industry 6:256–262
42. Gu J, Zhang H, Zhang J, Wen C, Zhou J, Yao H, He Y, Ma H, Duan Y (2020) Optimization, characterization, rheological study and immune activities of polysaccharide from *Sagittaria sagittifoliaL.*. Carbohydr Polym 246:116595
43. Mason TJ (2015) Some neglected or rejected paths in sonochemistry–a very personal view. Ultrason Sonochem 25:89–93
44. Rouhani M (2019) Modeling and optimization of ultrasound-assisted green extraction and rapid HPTLC analysis of stevioside from *Stevia Rebaudiana*. Ind Crops Prod 132:226–235
45. Khadhraoui B, Turk M, Fabiano-Tixier AS, Petitcolas E, Robinet P, Imbert R, Maataoui ME, Chemat F (2018) Histo-cytochemistry and scanning electron microscopy for studying spatial and temporal extraction of metabolites induced by ultrasound. Towards chain detexturation mechanism. *Ultrason Sonochem* 42:482–492
46. Santos KA, Gonçalves JE, Cardozo-Filho L, da Silva EA (2019) Pressurized liquid and ultrasound-assisted extraction of α-bisabolol from candeia (*Eremanthus erythropappus*) wood. Ind Crops Prod 130:428–435
47. Plaza M, Turner C (2015) Pressurized hot water extraction of bioactives. TrAC, Trends Anal Chem 71:39–54
48. Lianfu Z, Zelong L (2008) Optimization and comparison of ultrasound/microwave assisted extraction (UMAE) and ultrasonic assisted extraction (UAE) of lycopene from tomatoes. Ultrason Sonochem 15(5):731–737
49. Alvarado-Morales G, Minjares-Fuentes R, Contreras-Esquivel JC, Montanez J, Meza-Velazquez JA, Femenia A (2019) Application of thermosonication for Aloe vera (*Aloe barbadensis* Miller) juice processing: impact on the functional properties and the main bioactive polysaccharides. Ultrason Sonochem 56:125–133
50. Ma Y, Ye X, Hao Y, Xu G, Xu G, Liu D (2008) Ultrasound-assisted extraction of hesperidin from Penggan (Citrus reticulata) peel. Ultrason Sonochem 15(3):227–232
51. Barbero GF, Liazid A, Palma M, Barroso CG (2008) Ultrasound-assisted extraction of capsaicinoids from peppers. Talanta 75(5):1332–1337
52. SeidiDamyeh M, Niakousari M, Saharkhiz MJ (2016) Ultrasound pretreatment impact on Prangos ferulacea Lindl and Satureja macrosiphonia Bornm essential oil extraction and comparing their physicochemical and biological properties. Industrial Crops and Products 87:105–115
53. Georgiadis N, Ritzoulis C, Sioura G, Kornezou P, Vasiliadou C, Tsioptsias C (2011) Contribution of okra extracts to the stability and rheology of oil-in-water emulsions. Food Hydrocolloids 25(5):991–999
54. Zhang Y, Wang C, Liu C, Wang X, Chen B, Yao L, Qiao Y, Zheng H (2020) Recent developments in stigma maydis polysaccharides: isolation, structural characteristics, biological activities and industrial application. Int J Biol Macromol 150:246–252
55. Natolino A, Da Porto C (2020) Kinetic models for conventional and ultrasound assistant extraction of polyphenols from defatted fresh and distilled grape marc and its main components skins and seeds. Chem Eng Res Des 156:1–12
56. Toda TA, Sawada MM, Rodrigues CEC (2016) Kinetics of soybean oil extraction using ethanol as solvent: experimental data and modeling. Food Bioprod Process 98:1–10
57. Oreopoulou A, Goussias G, Tsimogiannis D, Oreopoulou V (2020) Hydro-alcoholic extraction kinetics of phenolics from oregano: optimization of the extraction parameters. Food Bioprod Process 123:378–389